



Contents lists available at ScienceDirect

Sensors and Actuators B: Chemical

journal homepage: www.elsevier.com/locate/snb

Electroosmotically driven microfluidic actuators

Menake E. Piyasena^a, Robert Newby^a, Thomas J. Miller^a, Benjamin Shapiro^b, Elisabeth Smela^{a,*}^a Department of Mechanical Engineering, University of Maryland, College Park, MD 20742, United States^b Department of Aerospace Engineering, University of Maryland, College Park, MD 20742, United States

ARTICLE INFO

Article history:

Received 2 April 2009

Received in revised form 8 May 2009

Accepted 11 May 2009

Available online xxx

Keywords:

Actuator
Elastomer
Microfluidics
Electroosmosis
PDMS
Smart material

ABSTRACT

A prototype electroactive polymer actuator has been developed based on electroosmotic (EO) pumping to create hydraulic pressure. The actuator was fabricated from poly(dimethylsiloxane) (PDMS) with embedded micro-scale channels, reservoirs, and electrodes surmounted by a membrane. An applied voltage caused one reservoir to expand as fluid was pumped into it, and the other reservoir to contract, with the membrane above the expansion reservoir rising by 400 μm within a few seconds. Since the prototype was made from PDMS, which is an elastomer, the device was entirely flexible. The actuator performance was characterized, and it agreed well with predicted values. Furthermore, the calculations indicate that, once optimized, such actuators could have high stress as well as high strain and high speed. By combining unit cells such as these into a material and actuating them individually via independently controlled flexible electrodes, one could realize smart materials that could change shape. Other future applications may include micro-valves, micro-positioners, soft robots, and active camouflage layers.

© 2009 Elsevier B.V. All rights reserved.

1. Introduction

The field of electroactive polymers (EAPs) is summarized in Fig. 1. It comprises thermally actuated devices, whether the actuation strain is due to the coefficient of thermal expansion (CTE) [1,2] or a change in phase [3]. It also includes electrostrictive polymer devices that respond directly to electric fields, such as dielectric elastomer actuators (DEAs) [4,5] and piezoelectric polymers [6]. The third family of devices are those in which strain is due to ion movement, including conjugated polymers (CPs) [7], gels [8–10], ionic polymer metal composites (IPMCs) [11], and carbon nanotube actuators [12]. In this paper, we describe a new type of actuator based on hydraulic pressure.

Moving liquids using electrical fields is routine in microfluidic systems [13–17]. The high surface-to-volume ratios in micro-scale systems mean that surface effects, such as those used in electroosmosis (EO), dominate over bulk effects and can create large forces [18–20]. (EO is the movement of liquid induced by an applied electric field.) EO pumps have been developed for a variety of applications, such as chip cooling [21] and fuel cell water evacuation [22]. However, there has been little prior work on electroosmotic pumping to produce mechanical work, aside from valving [23–26]. Since EO can produce mechanical deformations with no mov-

ing parts, it is attractive to consider using it for micro-system actuation.

The mechanism for EO pumping is the following. Upon immersing a solid into a fluid, a net charge is created at the interface due to adsorption of ions or due to protonation or deprotonation of surface groups [27]. A charge-compensating Debye layer made up of mobile ions therefore builds up in the fluid. The resulting electric field at the interface is characterized by the zeta potential. A voltage applied along the channel, i.e. parallel to the walls, acts on the mobile ions near the walls, and these in turn drag the fluid in the channel.

The term *nastic* is used in botany to mean a movement in response to a stimulus, such as a change in turgor, or cell pressure. The hydrostatic cell pressure in plants is determined by the water content. In the actuator introduced in this paper, the water content in different parts of the microfluidic cell is controlled by EO pumping. Therefore, in analogy with the way that plants move by hydraulic actuation, we dub these devices “nastic actuators.”

The concept of the hydraulic, EO-driven nastic actuator is illustrated in Fig. 2A and B. The actuation cell contains a fluid supply reservoir chamber, a smaller expansion chamber, and micro- or nano-channels connecting the two. Electrodes ending in the two chambers are connected to a voltage supply. The application of an electric field creates electroosmotic pumping in each of the microchannels. This causes the expansion chamber to fill with additional fluid, and thus the flexible material forming the actuator cell to deform, until the point at which the material's elastic restoring force or the external load balances the pressure created in the chan-

* Corresponding author at: Department of Mechanical Engineering, University of Maryland, 2176 Glenn L. Martin Hall, College Park, MD 20742, United States. Tel.: +1 301 405 5265; fax: +1 301 314 9477.

E-mail address: smela@umd.edu (E. Smela).

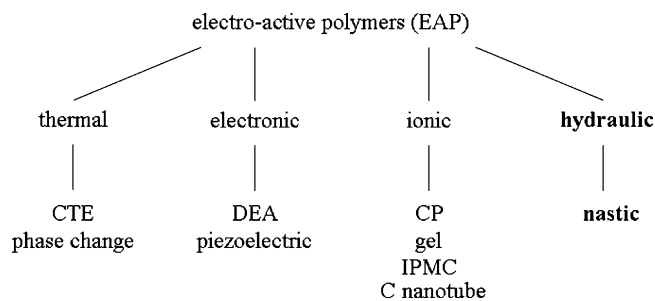


Fig. 1. Overview of the types of EAP.

nels. Multiple channels connected in parallel increase the flow rate, and hence the actuation speed.

In this paper, we show proof of concept for such an actuator, demonstrate that it can be produced using standard soft lithography techniques, and show that the performance is consistent with that expected theoretically. We then suggest potential applications and future work.

2. Experimental

Soft lithographic techniques were used to build the prototype devices. Masks for lithography were drawn using AutoCAD (Autodesk, San Rafael, CA) and printed commercially (CADArt Service, Bandon, OR) at high resolution (20,000 dpi). The expansion reservoir was 2.5 mm × 5.0 mm and the supply reservoir was 5.0 mm × 5.0 mm. They were connected by nine channels that were 1 cm long and 150 μm wide.

Molds for the PDMS structures were formed of SU8-2050 (a negative photoresist, Microchem, Newton, MA). The SU8 was spin-coated onto a 3 in. silicon wafer at 500 rpm for 5 s with 100 rpm/s acceleration, and then at 2000 rpm for 1 min with 100 rpm/s acceleration. The wafer was pre-baked at 65 °C for 5 min and then at 95 °C for 15 min with a 300 °C/h ramp on a hot plate. The sample was cooled to room temperature over 10 min. The SU8 was exposed to UV light (9 mJ/cm²) for 20 s through the mask, then baked at 65 °C for 1 min and 95 °C for 6 min. The pattern was developed in SU-8 developer (Microchem, Newton, MA) to produce the mold. Thicknesses were measured by profilometry (Alphastep 200). The final mold had an average depth of 60 μm.

The mold substrate was placed into a Petri dish. Two thin metal rods 2 cm long and 0.5 mm in diameter were placed vertically at the centers of the two reservoir locations on the mold and held in place using two rare earth magnets underneath the wafer. A silicone tube (2.5 cm long, 0.89 mm I.D., Cole Parmer, Vernon Hills, IL) was placed around each rod. The rods held the tubes upright and in place during PDMS curing.

The PDMS pre-polymer solution and curing agent (Sylgard 184 R, Dow Corning) were mixed at a ratio of 10:1 (w/w), then degassed in a vacuum desiccator for 30 min to eliminate air bubbles. The mixture was poured onto the mold to a height of 2 mm and baked at 70 °C for 1 h in an oven. The PDMS layer was peeled off of the mold, and the two metal rods were removed from inside the silicone tubes, the outer sides of which had bonded to the PDMS. At the same time, some of the PDMS mixture was spin-coated onto a glass slide at 2000 rpm for 1 min to produce a 25-μm thick PDMS membrane. The film on the glass slide was baked at 95 °C for 15 min on a hot plate.

To seal them together irreversibly, the PDMS film with the reservoirs, channels, and tubing, and the PDMS membrane on the glass slide were both treated with O₂ plasma for 8 s at 700 mTorr and 35 W in a reactive ion etcher. The two surfaces were brought into contact and allowed to rest for an hour. The channel depth after seal-

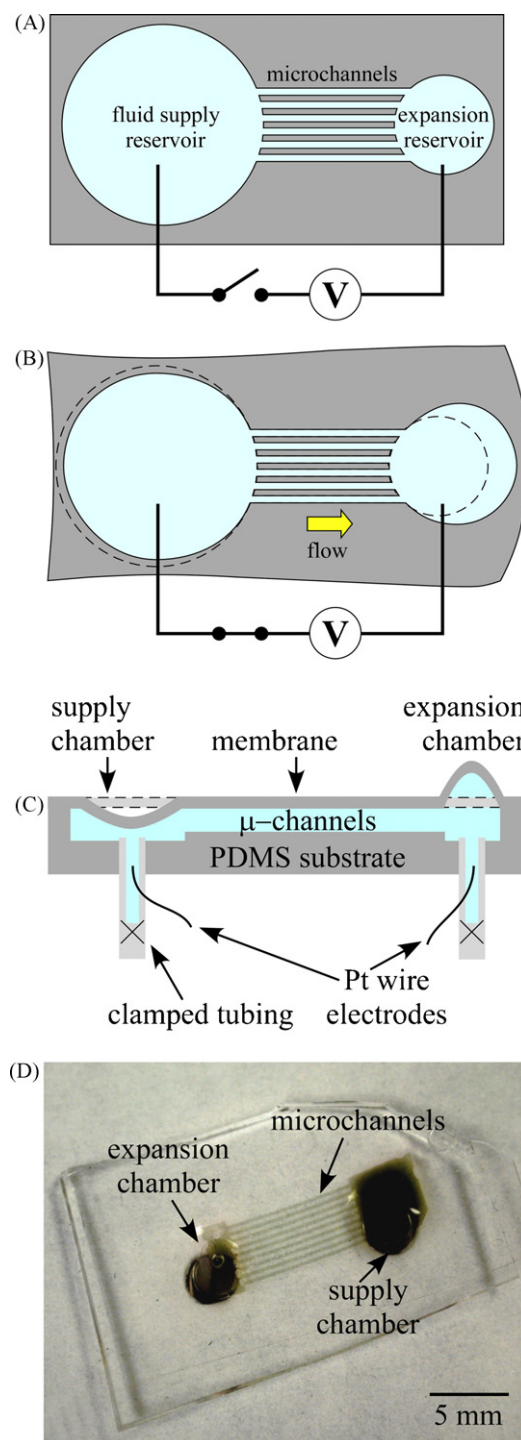


Fig. 2. (A) Schematic overhead view of an actuation cell with the voltage off. (B) Electroosmotically pumping the fluid from left (anode, +) to right (cathode, -) causes the expansion reservoir to expand. (C) Schematic cross-sectional view of the prototype nastic device. (D) Top view photograph of the prototype device filled with water (dyed brown for visualization). (For interpretation of the references to color in this figure legend, the reader is referred to the web version of the article.)

ing was measured using optical microscopy and was determined to be 25 μm.

Two 3 cm long, 0.25 mm diameter Pt wires were inserted through the sidewalls of the silicone tubes. The holes were sealed with a UV curable adhesive (Loctite 3525, Henkel North America) to prevent leakage during device operation. The electrode in the supply reservoir later served as the anode, and the one in the expansion

sion reservoir as the cathode to pump fluid from the former to the latter.

The assembled device was peeled off the glass slide and filled with pump fluid via a syringe pump (NE-1000, New Era Pump Systems Inc., Wantagh, NY) connected to the tube at the expansion reservoir. Deionized (DI) water served as the pumping fluid in these experiments. It was pumped through the device for several minutes to remove trapped air. The silicone tubes were then clamped shut, and the two Pt electrodes were connected to a high voltage power supply (Ultravolt HV Rack, Ultravolt, Ronkonkoma, NY). A side view schematic of the final device is shown in Fig. 2C, and an actual device in Fig. 2D. Before each run (i.e. the collection of a data point or a curve in the plots), the chambers and microchannels were rinsed and filled with fresh DI water and visually inspected for the presence of air bubbles in the system.

Actuation was recorded using a digital video camcorder (Sony Digital Handycam). Still images were taken through the microscope using a digital camera (Nikon Coolpix 4500). Deflection was measured using a force/strain transducer (Aurora 400B, Ontario, Canada). The transducer was interfaced to a PC via a data acquisition card (National Instruments), and data were recorded using a custom LabVIEW program.

During isotonic measurements to measure the deflection under different applied loads, the force/strain transducer arm rested on the actuator. To distribute the load from the force/strain transducer arm more uniformly over the membrane, a 2 mm × 4 mm piece of plastic transparency film was placed between the membrane over the expanding chamber and the transducer arm. The tip of the arm pushed downward, and the deflection was measured versus voltage for different loads. The area of the transparency in contact with the membrane decreased as the reservoir inflated, spreading the load over a smaller area. In isometric measurements to measure blocked force, the arm was held in a fixed position just above the actuator with the membrane uninflated, and the force was mea-

sured versus voltage. The force was thus distributed over the entire 2.5 mm × 5 mm area.

All measurements were performed in randomized order to remove systematic error. A separate device was used for each of the characterization plots. Before use, devices were tested by measuring the membrane deflection using the force/strain transducer under an applied voltage of 5 kV. Deflections of $180 \pm 20 \mu\text{m}$ were consistently reached, and devices that deviated more than this were considered to be defective and were not used. A small number of measurements were taken at 10 kV, but since this resulted in considerable bubble generation due to hydrolysis and could also lead to electrical arcing, voltages were usually kept to 7.5 kV and below.

3. Results

A schematic of the prototype actuator is illustrated in Fig. 2C, and one of the actual prototypes is shown in Fig. 2D. For these experiments, the pumping fluid was deionized water. Upon application of a high voltage to this device, the PDMS membrane over the expansion reservoir deflected upward (Fig. 3), while the membrane over the supply reservoir deflected downward slightly. Deflection increased with applied voltage, and at 10 kV a substantial deflection of 400 μm was achieved at the center of the membrane. (While the voltage is high, the current is low; voltages of this magnitude are routinely used in the actuator and EO fields [4,20,28].)

At the beginning of actuation with fresh fluid, the current was relatively high (10–50 μA), but then decreased (to 1 μA) within 5–10 s and thereafter remained relatively stable (>30 min). The characterization reported below was performed after the current had stabilized.

Characterization of the actuator's performance focused on the response under different voltages and mechanical loads. The deflection as a function of voltage is shown for two devices under two different isotonic loads in Fig. 4A. Deflection was linear with volt-

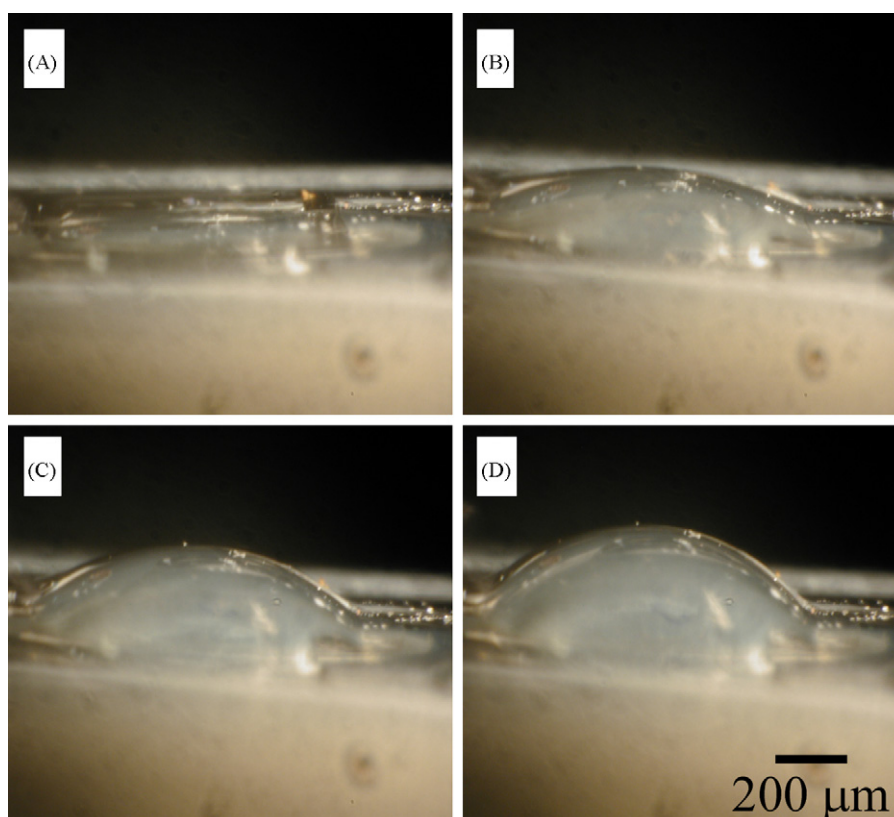


Fig. 3. Optical micrographs of actuation at different voltages: (A) 0 kV, (B) 1 kV, (C) 5 kV, and (D) 10 kV.

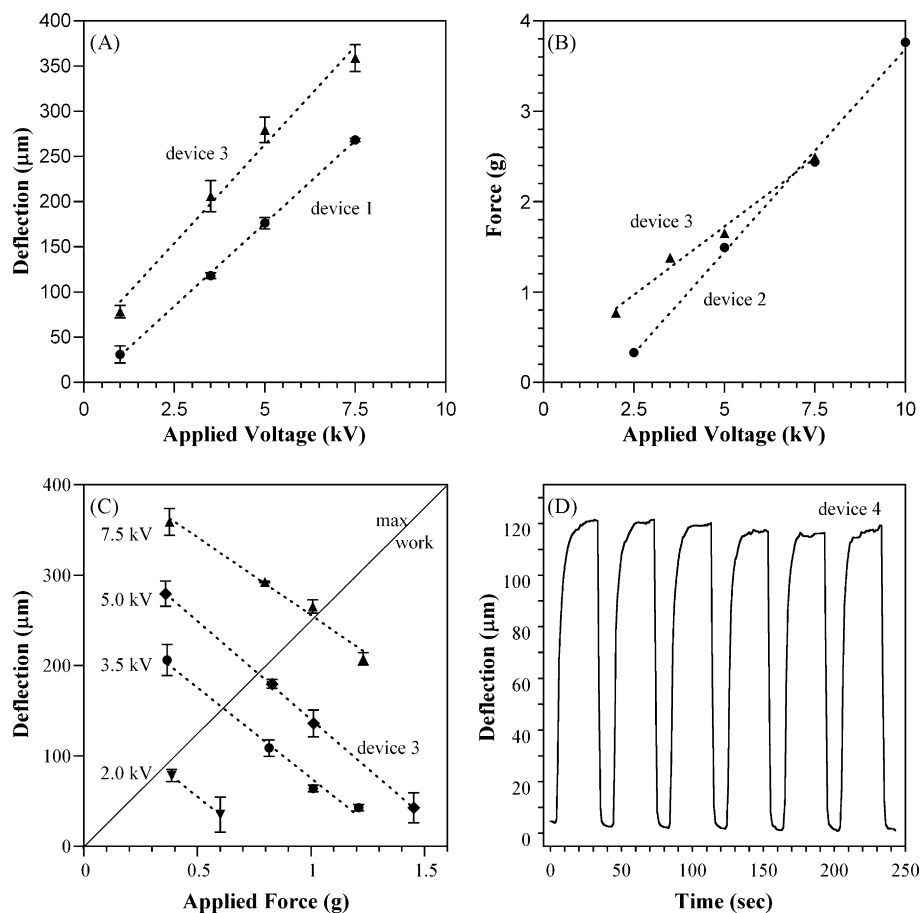


Fig. 4. (A) Deflection as a function of voltage under loads of 0.65 g (device 1) and 0.36 g (device 3). (Data points with error bars represent an average of three replicates.) (B) Force as a function of applied voltage. (C) Deflection under various applied forces (load lines). (D) Deflection vs. time upon stepping the voltage between 3.5 kV and off.

age, reaching 270 μm at an applied voltage of 7.5 kV under a load of 0.65 g for device 1 and 360 μm under a load of 0.36 g for device 3. The blocked force generated by the actuators is shown as a function of voltage in Fig. 4B. These lines were also linear, with device 2 reaching 3.7 g at 10 kV. (The minor difference in the two sets of data may be due to slight variations in membrane thicknesses, the presence of micro-scale air bubbles, or changes in pH.)

For many applications, including load-carrying micro-robots, it is important to know the distance that a given weight can be lifted by the device. The deflections under load (isotonic, from 0.35 to 1.45 g, device 3) were measured for various voltages as shown in Fig. 4C, yielding a set of linear load curves. Work, defined as force \times distance, is maximized along the diagonal line shown in the figure. (A plot of the work is included in the Supporting Information.) Extrapolating the load curves to a force of 0 gives the free strain, and extrapolating to a deflection of 0 gives the blocked force. This was done to obtain the device 3 curve in Fig. 4B, and the results are comparable to isometric measurements of blocked force on device 2.

Speed and reproducibility are also critical in micro-actuators, particularly for applications such as micro-positioning and on/off valving. These performance metrics were tested by repeatedly stepping the voltage on/off (Fig. 4D). The maximum displacement (120 μm under 3.5 kV and 0.7 g, device 4) was obtained within 15 s (80% of maximum deflection was reached within 5 s, 94% within 10 s), whereas full collapse was reached in only 2–3 s. The extent and speed of deflection and collapse were reproducible throughout these measurements (50 cycles, of which only 6 are shown).

4. Theory

The volume flow rates determine how quickly the expansion chamber fills and empties, and thus the actuation speed. The EO pumping flow rate \dot{v} for n rectangular channels during filling of the chamber is given by

$$\dot{v} = nwd \frac{\varepsilon \varepsilon_0 \zeta |\bar{E}|}{\eta}, \quad (1)$$

where w is the width of the channels and d is their depth, ε is the dielectric constant of the liquid, ε_0 is the permittivity of free space, ζ is the zeta potential, \bar{E} is the electric field, and η is the viscosity of the liquid. The zeta potential varies according to both the liquid and solid materials and the surface preparation; for native PDMS this is typically on the order of 0.1 V. For our system, at 3.5 kV we would expect a flow rate of 0.65 $\mu\text{L/s}$ for $\zeta = 0.1$ V under free flow conditions without opposing force. (All calculations are shown in the Supporting Information.) Experimentally, we obtained a value of 0.13 $\mu\text{L/s}$ (for a normalized flow rate of 2.8 $\mu\text{L}/\text{min V cm}^2$) during the first 5 s under the opposing force of the membrane, which is a typical EO flow rate [26]. Using $\zeta = 0.05$ V in Eq. (1) gives 0.14 $\mu\text{L/s}$. The flow rate can most readily be increased by increasing the number and depth of channels, since the flow rate depends linearly on the cross-sectional channel area $A = nwd$. Note that because there are numerous channels, the device will continue to function even if one or more of the channels becomes clogged.

For pressure-driven flow in a rectangular channel, such as occurs when the PDMS relaxes and the expansion reservoir empties, the

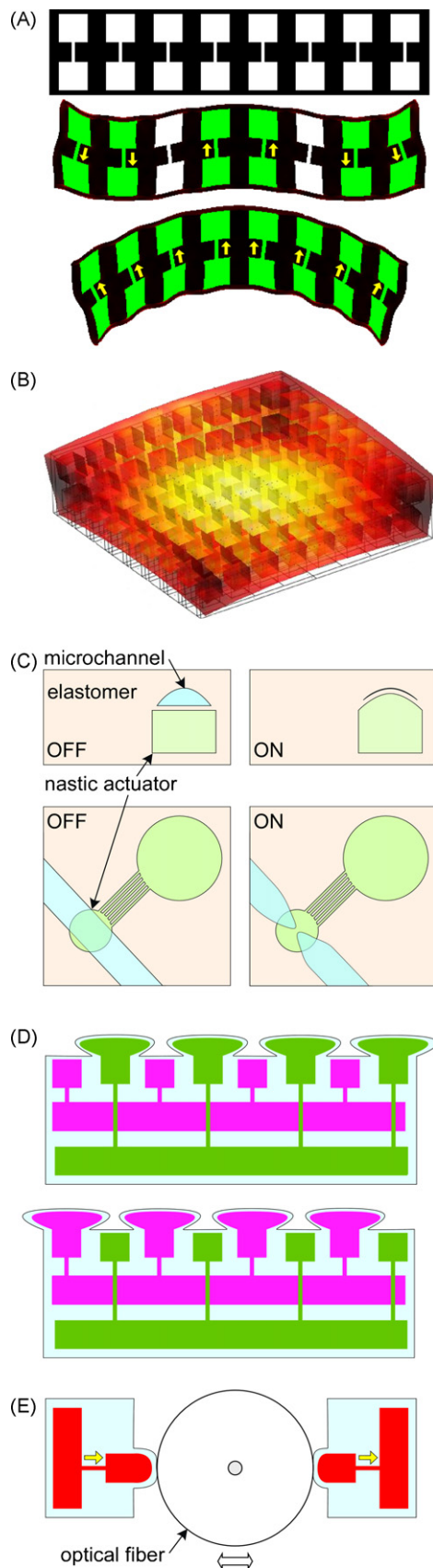


Fig. 5. Potential future applications of nastic actuators. (A) Simulation results showing bending and rippling of a strip upon actuation (green cells are active, white cells are off). (B) Simulation results (see Supporting Information for details) showing cupping of a sheet comprising a 2D array of nastic cells. (C) Schematic of a micro-valve shown in cross-sectional and overhead views. (D) Possible design for

flow rate can be found approximately by [29]

$$\dot{v} = n \frac{d^3 w}{12 \eta L} \Delta P \left[1 - 0.63 \frac{d}{w} \right], \quad (2)$$

where the pressure drop ΔP is provided by the elastic restoring force of the elastomer and any external load, and L is the length of the channels. Since the approximate flow rate during relaxation is known ($0.39 \mu\text{L/s}$ from the data in Fig. 4D; see the Supporting Information) the restoring pressure ΔP can be calculated and is found to be equal to 2500 Pa.

The maximum actuation stress that can be achieved by the EO flow is

$$P = \frac{12 l \epsilon \epsilon_0 \zeta \left| \vec{E} \right|}{d^2 \left[1 - 0.63 d/w \right]} \quad (3)$$

This relationship shows that higher pressures can be achieved by making the channels smaller, since that leads to larger surface-to-volume ratios. For channels with diameters on the order of tens of nm, stresses on the order of tens to hundreds of GPa are theoretically possible in optimized devices. Pressures in excess of 20 MPa have already been achieved experimentally using electroosmotic flows in micro-capillaries packed with silica micro-particles [28]. The pressure can also be increased by increasing the zeta potential, the dielectric constant of the fluid, and the voltage.

Note that the pressure should be linear with the applied voltage, which is what was found in Fig. 4. In our geometry, the calculated pressure is 870 Pa under a voltage of 3.5 kV (0.25 Pa/V) for $\zeta = 0.05 \text{ V}$. It should be possible to increase this value by 5 orders of magnitude by decreasing channel dimensions, for example by using micro/nanoporous frits [26]. This 870 Pa pressure, taken over the area of the reservoir, should be able to lift a weight of 1.1 g. This is the same as the 1.2 g of blocked force that was observed experimentally at this voltage (Fig. 4C).

The deflection y of a thin membrane (held plate, large deflections) due to a pressure P can be approximated by [30]

$$P = \frac{\pi^6}{64} \left\{ 4Dy \left(\frac{1}{a^2} + \frac{1}{b^2} \right)^2 + \frac{Ety^3}{4} \left(\frac{1}{a^4} + \frac{1}{b^4} \right) + \frac{Ety^3}{2(1-\nu^2)} \left[\frac{2}{a^2 b^2} + \nu \left(\frac{1}{a^4} + \frac{1}{b^4} \right) \right] \right\}, \quad (4)$$

where D is the flexural rigidity, a is half the length of the membrane, b is half its width, E is its Young's modulus, t is its thickness, and ν is the Poisson ratio. Solving for y for an actuation pressure of 870 Pa gives a deflection of $240 \mu\text{m}$. Extrapolating the 3.5 kV line in Fig. 4C to 0 g gives $280 \mu\text{m}$. The deflection prediction is thus spot on, given the experimental uncertainties.

One potential problem is rupturing the reservoir when too high a pressure is applied. The maximum deflection of the membrane is limited by the ultimate tensile stress σ_U and the ultimate tensile strain ϵ_U of the material. These depend on the precursor to hardener ratio used during preparation, the curing temperature, and the film thickness, but σ_U is typically 2–20 MPa [31–35]. As the deflection of the membrane increases, the tensile stress begins to dominate the bending stress [30,36]. Neglecting the bending stress, the tensile stress at the center of a uniformly loaded circular membrane of radius a clamped at the edges is [36]

$$\sigma = 0.423 \left(\frac{EP^2 a^2}{t^2} \right)^{1/3}. \quad (5)$$

a color-changing material. (E) Concept for a micro-positioning system, shown here for optical fibers.

Substituting $\sigma_{ij} = 2$ MPa for σ and using half the length of the longest edge of the reservoir for a , the maximum pressure that the membrane can withstand can be estimated as approximately 0.1 MPa, 2 orders of magnitude higher than seen in our device. Making the membrane twice as thick would double the permissible pressure but reduce the deflection by 52 μm , to 187 μm while halving the membrane thickness would halve the pressure but increase the deflection by 63 μm , to 302 μm . Looking now at the ultimate tensile strain, for a deflection of 240 μm , the membrane is stretched along the short axis of the reservoir by only 2.4% (see [Supporting Information for details](#)), far below the experimentally determined ultimate tensile strain of $\sim 80\%$ for this formulation of PDMS. A strain of 80% is reached for a vertical deflection somewhat greater than 1.25 mm.

The fact that the experimental performance and the theoretical predictions are close on all of the measures above gives us good reason to believe that, as predicted theoretically, nastic actuators will be able to exert both significant actuation stresses and strains, and that the speeds will be reasonable for the envisioned applications. In fact, the stress and strain achievable with this technology, once optimized, could potentially exceed the performance of all competing micro-technologies.

5. Discussion

The prototype nastic actuator comprised only a single expansion chamber. One can imagine, however, integrating together many cells with different sizes and orientations to create a *smart material*, which could, in principle, be meso-scale or even macro-scale [37]. Simulation results for a strip of 8 cells and for a sheet containing 8×8 cells are shown in [Fig. 5A](#) and [B](#). By independently actuating the cells, one would be able to obtain complex motions, enabling the strip to walk like an inchworm or grasp and manipulate an object like an octopus tentacle, or enabling the sheet to swim like a jellyfish. In other words, one would be able to create a soft robot. There is considerable design freedom with this technology since one can vary the shapes of the reservoirs and the channels, their orientations and their connectivity [38], and also the elastomer's stiffness.

Another possible application of nastic actuators would be in micro-valves ([Fig. 5C](#)), inspired by Quake's micro-valves [39], but completely miniaturizable since no external hydraulic system is required. These would be of interest for handheld systems or even for integration into disposable devices. Another possibility is color-changing chameleon surfaces ([Fig. 5D](#)), which would work by pumping various colored fluids to the surface, expanding or contracting the areas of color displayed. These programmable pixels would be analogous to chromatophores in cuttlefish skin, which control the area of a pigmented sac [40]. Multiple layers and colors can be envisioned, although only two are shown here. The actuators could finally also be used as large-strain micro-positioners. A positioner for aligning optical fibers is illustrated in [Fig. 5E](#), in which the expansion/contraction of opposing chambers would push the fiber right or left, with the elastomers providing some grip.

There are a number of significant challenges that will need to be faced to realize the potential applications suggested in [Fig. 5](#). First, the number of channels should be increased while their size should be decreased in order to improve the actuation stress but retain the flow rate. One promising approach is to utilize porous polymer materials [25,41], the pores serving as the desired multiple nano-scale channels. Second, hydrolysis needs to be addressed: under the high voltages applied in the prototype, the water splits, creating gas bubbles and changing the pH, and thus changing the zeta potential and the pumping characteristics. Thus, holding the pumping voltage on for long time periods results in unpredictable fluctua-

tions in current, and thus membrane deflection (see the [Supporting Information](#)). It has been shown that bubble formation can be suppressed, for example by using a catalyst to recombine the gases into water [19], employing palladium as the electrode material [26], and/or using salt bridges [42]. The use of redox couples can also be explored since they have been shown to allow EO at high pressure without gas generation [43]. AC electroosmosis [26] can also help with electrode and pumping fluid stability. Alternatively, an organic solvent may be a better choice than water for the pumping fluid. However, since PDMS swells in many organic solvents, leading to device leakage and slow evaporation, the elastomer may need to be changed. Highly crosslinked fluorinated polymers are a possibility for the elastomer, since these materials have been shown to have good solvent compatibility [44]. Third, the device needs to be further miniaturized by removing the tubes and the wire electrodes. This requires a method of filling the device with fluid, for example using a syringe needle. This also requires flexible electrodes that are stable to corrosion. Fourth, the device should be further optimized by adjusting the surface wall coating to achieve a larger and more uniform zeta potential. It is our hope that the success of the first EOF-based nastic actuator reported here will inspire creative solutions to these challenges, as well as the creation of new "soft" devices and systems.

6. Conclusions

This paper has demonstrated a novel electroactive polymer actuator based on hydraulic pressure. It was enabled by taking advantage of an effect that works on the micro-scale but not the macro-scale: electroosmotic pumping, in which fluid is pumped within microfluidic systems by the application of an electric field. The first (unoptimized) prototype already demonstrated good performance, with a displacement of hundreds of μm within seconds. The performance of the device followed the theoretical predictions, which indicates that upon optimization, high actuation forces can be achieved as well. Further, numerous applications can be envisioned, including soft robotics, micro-valves, and micro-positioners.

Acknowledgements

We thank Jason West for modeling the multi-cell devices in [Fig. 5](#). Funding was provided by the University of Maryland's Minta Martin Aeronautical Research Fund. We acknowledge the support of the Maryland NanoCenter and would like to thank the staff of the clean room (FabLab). We also thank Santa Fe Science and Technology for the donation of the force/strain transducer and the LabVIEW program used in its operation.

Appendix A. Supplementary data

Supplementary data associated with this article can be found, in the online version, at [doi:10.1016/j.snb.2009.05.014](https://doi.org/10.1016/j.snb.2009.05.014).

References

- [1] M. Ataka, A. Omodaka, N. Takeshima, H. Fujita, Fabrication and operation of polyimide bimorph actuators for a ciliary motion system, *J. Microelectromech. Syst.* 2 (4) (1993) 146.
- [2] T. Ebefors, E. Kälvesten, G. Stemme, Dynamic actuation of polyimide V-groove joints by electrical heating, *Sens. Actuat. A* 67 (1998) 199–204.
- [3] A. Buguin, M.-H. Li, P. Silberzan, B. Ladoux, P. Keller, Micro-actuators: when artificial muscles made of nematic liquid crystal elastomers meet soft lithography, *J. Am. Chem. Soc.* 128 (2006) 1088–1089.
- [4] R. Pelrine, R. Kornbluh, Q.B. Pei, J. Joseph, High-speed electrically actuated elastomers with strain greater than 100%, *Science* 287 (5454) (2000) 836–839.
- [5] M. Aschwanden, A. Stemmer, Polymeric, electrically tunable diffraction grating based on artificial muscles, *Opt. Lett.* 31 (17) (2006) 2610–2612.

- [6] T.B. Xu, Z.Y. Cheng, Q.M. Zhang, High-performance micromachined unimorph actuators based on electrostrictive poly(vinylidene fluoride-trifluoroethylene) copolymer, *Appl. Phys. Lett.* 80 (6) (2002) 1082–1084.
- [7] E. Smela, O. Inganäs, I. Lundström, Controlled folding of micrometer-size structures, *Science* 268 (June) (1995) 1735–1738.
- [8] Y. Osada, Conversion of chemical into mechanical energy by synthetic polymers (chemomechanical systems), *Adv. Polym. Sci.* 82 (1987) 1–46.
- [9] T. Kaneko, T. Miyazaki, K. Yamaoka, Y. Katayama, A. Matsuda, J.P. Gong, Y. Osada, Shape memory gels with multi-stimuli-responses, *Smart Structures and Materials 1999: Electroactive Polymer Actuators and Devices*, Newport Beach, CA, USA, March 1–2, 1999, pp. 199–208.
- [10] D.J. Beebe, J.S. Moore, J.M. Bauer, Q. Yu, R.H. Liu, C. Devadoss, B.-H. Jo, Functional hydrogel structures for autonomous flow control inside microfluidic channels, *Nature* 404 (April) (2000) 588–590.
- [11] M. Shahinpoor, Y. Bar-Cohen, J.O. Simpson, J. Smith, Ionic polymer–metal composites (IPMCs) as biomimetic sensors, actuators and artificial muscles—a review, *Smart Mater. Struct.* 7 (1998) R15–R30.
- [12] R.H. Baughman, C. Cui, A.A. Zakhidov, Z. Iqbal, J.N. Barisci, G.M. Spinks, G.G. Wallace, A. Mazzoldi, D. de Rossi, A.G. Rinzler, O. Jaschinski, S. Roth, M. Kertesz, Carbon nanotube actuators, *Science* 284 (May) (1999) 1340–1344.
- [13] D.J. Harrison, K. Fluri, N. Chiem, T. Tang, Z.H. Fan, Micromachining chemical and biochemical analysis and reaction systems on glass substrates, *Sens. Actuat. B* 33 (1–3) (1996) 105–109.
- [14] G.J.M. Bruin, Recent developments in electrokinetically driven analysis on microfabricated devices, *Electrophoresis* 21 (18) (2000) 3931–3951.
- [15] D.J. Laser, J.G. Santiago, A review of micropumps, *J. Micromech. Microeng.* 14 (6) (2004) R35–R64.
- [16] T. Bayraktar, S.B. Pidugu, Characterization of liquid flows in microfluidic systems, *Int. J. Heat Mass Transf.* 49 (5–6) (2006) 815–824.
- [17] H.A. Stone, A.D. Stroock, A. Ajdari, Engineering flows in small devices: microfluidics toward a lab-on-a-chip, *Annu. Rev. Fluid Mech.* 36 (2004) 381–411.
- [18] M.E. Piyasena, G.P. Lopez, D.N. Petsev, An electrokinetic cell model for analysis and optimization of electroosmotic microfluidic pumps, *Sens. Actuat. B* 113 (1) (2006) 461–467.
- [19] S. Yao, D.E. Hertzog, S. Zeng, J.C. Mikkelsen Jr., J.G. Santiago, Porous glass electroosmotic pumps: design and experiments, *J. Colloid Interface Sci.* 268 (2003) 143–153.
- [20] S. Zeng, C.-H. Chen, J.C. Mikkelsen Jr., J.G. Santiago, Fabrication and characterization of electroosmotic micropumps, *Sens. Actuat. B* 79 (2–3) (2001) 107–114.
- [21] S.E. Kim, R.S. List, J.G. Maveety, A.M. Myers, Q.T. Vu, R. Prasher, R. Mahajan, G. Vandentop, Using external radiators with electroosmotic pumps for cooling integrated circuits, *US Patent* 6,992,381 (2006).
- [22] J.G. Santiago, J. Posner, F.B. Prinz, T. Fabian, J. Eaton, S. Cha, C. Buie, D. Kim, H. Tsuru, J. Sasahara, T. Kubota, Y. Saito, Fuel cell with electroosmotic pump, *US Patent* US 2006/0029851 A1 (2006).
- [23] P.H. Paul, D.J. Rakestraw, Electrokinetic high pressure hydraulic system, *US Patent* 6,019,882 (2000).
- [24] J. Krumme, Valve for controlling flow of a fluid, *US Patent* (2007).
- [25] B.J. Kirby, T.J. Sheppard, E.F. Hasselbrink Jr., Voltage-addressable on/off microvalves for high-pressure microchip separations, *J. Chromatogr. A* 979 (2002) 147–154.
- [26] A. Brask, D. Snakenborg, J.P. Kutter, H. Bruus, AC electroosmotic pump with bubble-free palladium electrodes and rectifying polymer membrane valves, *Lab Chip* 6 (2) (2006) 280–288.
- [27] K.V. Sharp, R.J. Adrian, J.G. Santiago, J.I. Molho, Liquid flows in microchannels, in: M. Gad-el-Hak (Ed.), *The MEMS Handbook*, CRC Press, Boca Raton, 2002, pp. 6.19–24.
- [28] L. Chen, J. Ma, Y. Guan, Study of an electroosmotic pump for liquid delivery and its application in capillary column liquid chromatography, *J. Chromatogr. A* 1028 (2) (2004) 219–226.
- [29] H. Bruus, *Theoretical Microfluidics*, Oxford University Press, New York, 2008, pp. 51.
- [30] D. Wang, A.I. El-Sheikh, Large-deflection mathematical analysis of rectangular plates, *J. Eng. Mech.* 131 (8) (2005) 809–821.
- [31] J.E. Mark (Ed.), *Polymer Data Handbook*, Oxford University Press, New York, 1999.
- [32] A. Mata, A.J. Fleischman, S. Roy, Characterization of polydimethylsiloxane (PDMS) properties for biomedical micro/nanosystems, *Biomed. Microdevices* 7 (4) (2005) 281–293.
- [33] P.W. Hum, Exploration of Large Scale Manufacturing of Polydimethylsiloxane (PDMS) Microfluidic Devices, BS Thesis, Mechanical Engineering, Massachusetts Institute of Technology, Boston, 2006.
- [34] M. Liu, J. Sun, Q. Chen, Influences of heating temperature on mechanical properties of polydimethylsiloxane, *Sens. Actuat. A* 151 (2009) 42–45.
- [35] M. Liu, J. Sun, Y. Sun, C. Bock, Q. Chen, Thickness-dependent mechanical properties of polydimethylsiloxane membranes, *J. Micromech. Microeng.* 035028 (2009).
- [36] S. Timoshenko, S. Woinowski-Krieger, *Theory of Plates and Shells*, 2nd ed., McGraw-Hill, New York, 1959.
- [37] B. Shapiro, E. Smela, Electrically driven microfluidic pumping for actuation, *US Patent* 7,523,608 B2 (2006).
- [38] M.E. Piyasena, B. Shapiro, E. Smela, A new EAP based on electroosmotic flow: nastic actuators, in: Y. Bar-Cohen (Ed.), *SPIE Smart Structures/NDE Electroactive Polymer Actuators and Devices (EAPAD) XI*, San Diego, CA, March 9–12, 2009, 7287, pp. 7287–59.
- [39] M.A. Unger, H.-P. Chou, T. Thorsen, A. Scherer, S.R. Quake, Monolithic microfabricated valves and pumps by multilayer soft lithography, *Science* 288 (April) (2000) 113–116.
- [40] E. Florey, Ultrastructure and function of cephalopod chromatophores, *Am. Zool.* 9 (2) (1969) 429–442.
- [41] J.A. Tripp, F. Svec, J.M.J. Frechet, S.L. Zeng, J.C. Mikkelsen, J.G. Santiago, High-pressure electroosmotic pumps based on porous polymer monoliths, *Sens. Actuat. B* 99 (1) (2004) 66–73.
- [42] Y. Takamura, H. Onoda, H. Inokuchi, S. Adachi, A. Oki, Y. Horiike, Low-voltage electroosmosis pump for stand-alone microfluidics devices, *Electrophoresis* 24 (1–2) (2003) 185–192.
- [43] P. Prakash, M.D. Grissom, C.D. Rahn, A.L. Zydney, Development of an electroosmotic pump for high performance actuation, *J. Membr. Sci.* 286 (1–2) (2006) 153–160.
- [44] B.J. Kirby, D.S. Reichmuth, R.F. Renzi, T.J. Sheppard, B.J. Wiedenman, Microfluidic routing of aqueous and organic flows at high pressures: fabrication and characterization of integrated polymer microvalve elements, *Lab Chip* 5 (2005) 184–190.

Biographies

Menake E. Piyasena is a postdoctoral research associate in the Department of Mechanical Engineering, at the University of Maryland, College Park. He received his BSc in Chemistry from the University of Kelaniya, Sri Lanka in 1997 and his PhD in Chemistry from the University of New Mexico in 2005. His interests include developing bead and cell-based microfluidic biosensors and electroosmosis-based applications in microfluidics.

Robert Newby is currently an undergraduate student in the Departments of Mechanical Engineering and Electrical and Computer Engineering at the University of Maryland. His research interests are related to MEMS and biological applications of MEMS.

Thomas J. Miller is currently an undergraduate student in the Department of Mechanical Engineering at the University of Maryland and will receive his BS in 2009, after which he intends to pursue an MS with Prof. Smela. His current fields of interests include micro-actuation and micro-robotics.

Benjamin Shapiro received a BS degree in Aerospace Engineering from the Georgia Institute of Technology in 1995 and a PhD degree in Control and Dynamical Systems from the California Institute of Technology in 1999. He is an Associate Professor in the Department of Aerospace Engineering at the University of Maryland, College Park. He is also affiliated with the Bioengineering Graduate Program and the Applied Math and Scientific Computation Program, and he is a member of the Maryland Nanocenter. His main interests are in modeling and control of micro-systems, with a primary focus on modeling and control of microfluidic systems for biochemical and medical applications.

Elisabeth Smela received her BS in Physics from MIT in 1985 and completed her PhD in Electrical Engineering at the University of Pennsylvania in 1992. She is an Associate Professor in the Department of Mechanical Engineering at the University of Maryland. She is an Affiliate of the Department of Electrical and Computer Engineering, a faculty of the Bioengineering Graduate Program, and a member of the Maryland Nanocenter. Her research interests are in artificial muscles, polymer MEMS, and bioMEMS, and more generally in combining organic materials with conventional inorganic materials to make new micro-scale devices.

Supporting Information

for

Nastic Actuators: Electroosmotically Driven Microfluidic Cells

Menake E. Piyasena, Robert Newby, Thomas J. Miller, Benjamin Shapiro, and Elisabeth Smela

The theoretical calculations for device performance are shown in detail in sections 1-5. In section 6 the experimental work done by the actuator is plotted as a function of applied force.

1 Variables

Table I. Variable values.

	Symbol	Values	Units	SI Value	SI Units
Device Dimensions					
<u>membrane-covered reservoirs</u>					
reservoir length	l_r	5.0	mm	5.00E-03	m
reservoir width	w_r	2.5	mm	2.50E-03	m
PDMS membrane thickness	h	25	μm	2.50E-05	m
round membrane equivalent radius	r	1.995	mm	1.995E-03	m
<u>channels</u>					
number of channels	n	9		9	
channel depth	d_c	60	μm	6.00E-05	m
channel width	w_c	150	μm	1.50E-04	m
channel length	l_c	1	cm	1.00E-02	m
<u>electrodes</u>					
distance between electrodes	L	3	cm	3.00E-02	m
Actuation					
applied voltage	V	3.5	kV	3,500	V
time required to inflate membrane	t_i	5	sec	5	sec
membrane deflection	h	120	μm	1.20E-04	m
time required to deflate membrane	t_d	2	sec	2	sec

Material Constants/Properties

dielectric constant of fluid	ϵ	78		78	
zeta potential	ζ	0.02	V	2.00E-02	V
viscosity of the liquid	η	0.001	N·s/m ²	1.00E-03	Pa·s
membrane Young's modulus	E_Y	0.5	MPa	5.00E+05	Pa
membrane Poisson's ratio	ν	0.4		4.00E-01	

Constants

permittivity	ϵ_0	8.9E-12	C ² /Nm ²	8.9E-12	C/Vm
gravitational constant	g			9.8	m/s ²

2 Flow Rate Due to EOF

2.1 Experimental EOF Flow Rate

To calculate the experimental flow rate, the volume of fluid in the membrane above the reservoir is divided by the time required to inflate the membrane. The volume V can be approximated as half the volume of a scalene ellipsoid

$$(1) \quad V = \frac{1}{2} \left(\frac{4}{3} \pi abc \right)$$

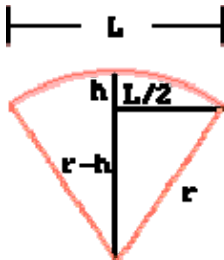
where a is half the length of the major axis ($l_r/2$), b is half the length of the minor axis ($w_r/2$), and c is the deflected height of the membrane. To obtain the flow rate over most of the inflation period, take the values to reach 80% of the final height of 120 μm (Figure 3D in the main text.) Using the values in Table I, for a deflection of $120 \mu\text{m} * 0.80 = 96 \mu\text{m}$,

$$(2) \quad V = 0.63 \mu\text{L}.$$

It takes 5 seconds to reach that height under an applied voltage of 3.5 kV, giving a flow rate of

$$(3) \quad Q_{EO} = dV/dt = 0.126 \mu\text{L}/\text{sec}.$$

To check this answer, one can also approximate the volume as the section of a hemisphere above the surface of the reservoir. The radius R of the circle, of which the expanded region is an arc, changes as the membrane inflates. It is related to the inflated height h and the diameter L as follows.



$$(4) \quad \begin{aligned} R^2 &= (R-h)^2 + L^2 / 4 \\ R^2 &= R^2 - 2Rh + h^2 + L^2 / 4 \\ 2Rh &= h^2 + L^2 / 4 \\ R &= \frac{h^2 + L^2 / 4}{2h} = \frac{4h^2 + L^2}{8h} \end{aligned}$$

To calculate the volume of the expanded area, integrate the area over the distance above the surface.

$$(5) \quad \begin{aligned} V &= \int_y^R \pi(R^2 - x^2) dx = \pi \left(R^2 x - x^3 / 3 \right) \Big|_y^R \\ &= \pi \left(R^3 - R^2 y - R^3 / 3 + y^3 / 3 \right) = \pi \left(\frac{2}{3} R^3 - R^2 y + y^3 / 3 \right) \end{aligned}$$

Setting $y = R - h$ and doing the algebra, we obtain

$$(6) \quad V = \frac{\pi}{3} (3Rh^2 - h^3).$$

Using an equivalent diameter of

$$(7) \quad r = \sqrt{ab / \pi}$$

and again using $h = 96 \mu\text{m}$ gives $V = 0.60 \mu\text{L}$. This is nearly the same as the volume as found above.

2.2 Theoretical EOF Flow Rate

The flow due to EOF is found by defining an electroosmotic mobility μ_{EO} [1]

$$(8) \quad \mu_{EO} = \frac{\varepsilon \varepsilon_0 \zeta}{\eta}$$

where ε is the dielectric constant, ε_0 is the permittivity, ζ is the zeta potential, and η is the fluid viscosity. The zeta potential depends on the chemistry of the fluid/channel wall system.

Applying an electric field \vec{E} produces an electroosmotic velocity v_{EO}

$$(9) \quad v_{EO} = \mu_{EO} |\vec{E}|$$

To obtain the flow rate, the velocity is multiplied by the cross sectional area A available for flow, which is the number of channels n times their width w_c and depth d_c .

$$(10) \quad Q_{EO} = Av_{EO} = nw_c d_c \frac{\varepsilon \varepsilon_0 \zeta}{\eta} |\vec{E}|$$

Using an estimate of $\zeta = 0.02 \text{ V}$, for an applied voltage of 3.5 kV we obtain

$$(11) \quad Q_{EO} = 0.13 \mu\text{L}/\text{sec}.$$

This is the same as the experimental value.

3 Flow Rate Due to Pressure

3.1 Experimental Pressure-Driven Flow Rate

When EOF is turned off, the elastic restoring forces of the membrane push the fluid back down. The time required to empty the reservoir, from a deflection of 120 μm (see Figure 3D), is two seconds. Calculating the fluid volume in the same manner as above gives $V = 0.785 \mu\text{L}$. This results in a relaxation flow rate Q_P of

$$(12) \quad Q_P = V/t = 0.393 \mu\text{L}/\text{sec}.$$

3.2 Theoretical Pressure-Driven Flow

3.2.1 Pressure Applied by the Membrane

The relationship between the flow rate Q_P and pressure difference ΔP for n rectangular channels due to a pressure gradient across the channels is [2]

$$(13) \quad Q_P = n \frac{d_c^3 w_c}{12\eta l_c} \Delta P \left[1 - 0.63 \frac{d_c}{w_c} \right]$$

where l_c is the length of the channel. Using the experimental relaxation flow rate, we can find the pressure on the membrane. Rearranging,

$$(14) \quad \Delta P = \frac{12\eta l_c}{n d_c^3 w_c} \frac{1}{\left[1 - 0.63 \frac{d_c}{w_c} \right]} Q_P$$

Using 0.393 $\mu\text{L}/\text{sec}$, we find a relaxation pressure of

$$(15) \quad \Delta P = 216 \text{ Pa}.$$

3.2.2 Pressure Due to EOF

By equating the flow rates due to EO, equation (10), and the membrane, equation (12), we can obtain the pressure due to EO flow, ΔP_{EO} .

$$(16) \quad \Delta P_{EO} = 12 l_c \varepsilon \varepsilon_0 \zeta \left| \bar{E} \right| / d_c^2 \left[1 - 0.63 \frac{d_c}{w_c} \right]$$

Note that this does not depend on the number of channels. Using the values in Table I we obtain

$$(17) \quad \Delta P_{EO} = 72 \text{ Pa}.$$

Since it took over 5 seconds to fill and 2 seconds to empty the fluid above the reservoir, we would have expected a pressure of less than approximately $216 * 2 / 5 = 86 \text{ Pa}$, which is consistent with the calculated value.

4 Membrane Deflection Due to EOF

The deflection y of the center of a rectangular membrane due to a pressure P is [3]

$$(18) \quad P = \frac{\pi^6}{64} \left\{ 4Dy \left(\frac{1}{a^2} + \frac{1}{b^2} \right)^2 + \frac{Ety^3}{4} \left(\frac{1}{a^4} + \frac{1}{b^4} \right) + \frac{Ety^3}{2(1-\nu^2)} \left[\frac{2}{a^2b^2} + \nu \left(\frac{1}{a^4} + \frac{1}{b^4} \right) \right] \right\}$$

where D is the flexural rigidity,

$$(19) \quad D = Et^3 / [12(1-\nu^2)],$$

E is the Young's modulus, and ν is the Poisson ratio. A pressure of 72 Pa is expected to produce a deflection of

$$(20) \quad y = 258 \mu\text{m}.$$

This is the same as the deflection of 280 μm observed experimentally at 3.5 kV.

5 Force Due to EOF

The area of the membrane is $A = w_r * l_r = 12.5 \text{ mm}^2$. The pressure is a force per unit area, so multiplying the pressure by the area should yield the force that can be exerted by the membrane. Experimentally, the blocking force for 3.5 kV was on the order of 1 gram. Using the area of the entire membrane, theoretically, we would expect

$$(21) \quad F = A * \Delta P_{EO} = 9 * 10^{-4} \text{ N}.$$

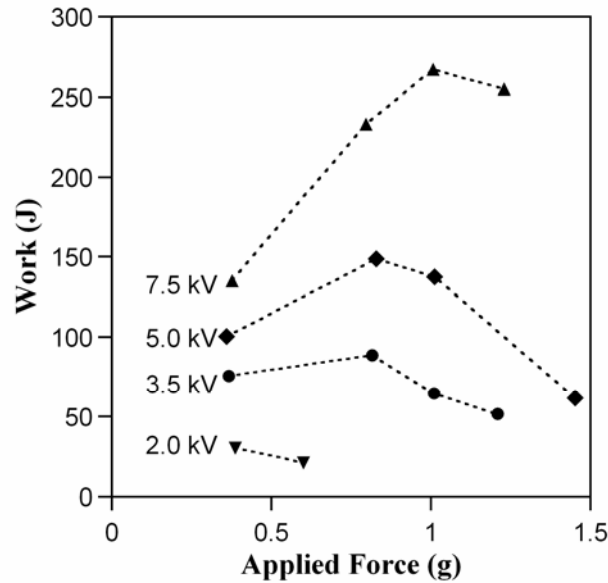
This corresponds to weight of

$$(22) \quad 9 * 10^{-4} \text{ N} / 9.8 \text{ m/sec}^2 = 0.09 \text{ g}$$

This value is too small by an order of magnitude. Given the fact that the contact area of the membrane with the polymer sheet on which the force/transducer arm rested was on the order of 1 mm^2 for a force of 1 g, the estimate is actually low by two orders of magnitude. This is quite surprising given the good agreement for the other values.

6 Work

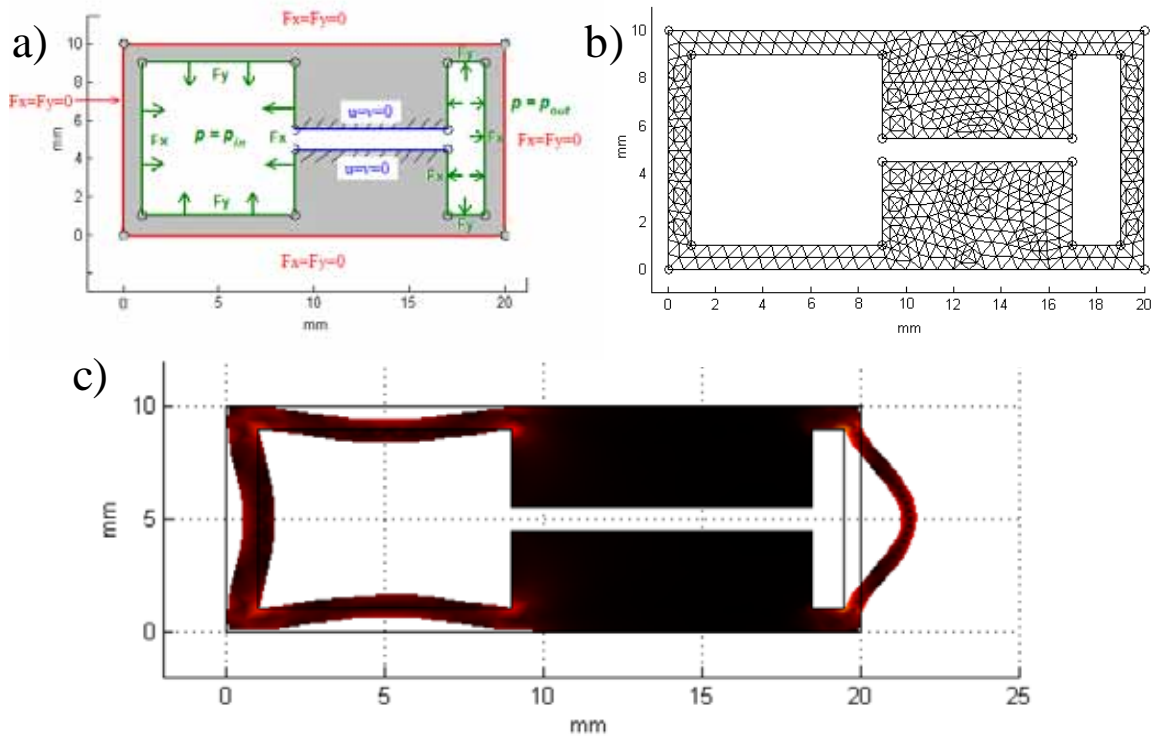
The work performed by the actuator at different applied voltages is shown here.



7 Simulations of Multi-Cell Deformations

Simulations of multi-cell material deformations, as shown in Figure 4A, B in the main text, were carried out as follows. For a single cell, the material was treated as linearly elastic. Equation (3) in the main text gave the pressure difference between the supply and expansion chambers. This pressure was applied as a boundary condition to the internal reservoir boundaries, as shown below. The resulting material deformation was assumed to be governed by standard elasticity equations and was computed using the multi-physics COMSOL software (www.comsol.com). COMSOL uses a finite element method and has a moving mesh capability that can keep track of large material deformations. A Lagrangian method was used wherein the mesh followed the motion of the material.

The figure below shows the model setup in two spatial dimensions for a single cell. The boundary conditions are shown in panel a): EO actuation creates a pressure difference in the reservoirs (pressure in on the left, pressure out on the right), the position of the channel is fixed (to prevent rigid body translations/rotations), and the free edges of the material have zero stress. Panel b) shows the mesh deforming with the material elements. Panel c) shows the resulting material deformation, colored by the von Mises stresses.



Simulations for a collection of cells, and for 3-dimensions, were done the same way, with the same boundary conditions repeated throughout. In the multi-cell simulations, two edge points were constrained to remain fixed in the y direction, and a center material point was constrained to remain fixed in the x direction; this allowed arbitrary deformation of the material but prevented rigid body translations and rotations.

8 References

- [1] J. P. Kutter, K. B. Mogensen, H. Klank, O. Geschke, "Microfluidics -- Components," in *Microsystem Engineering of Lab-on-a-chip Devices* (Eds: O. Geschke, H. Klank, P. Telleman) Wiley-VCH, Weinheim, **2004**, p. 39-77.
- [2] H. Bruus, *Theoretical Microfluidics*, Oxford University Press, New York, **2008**, p. 51.
- [3] D. Wang, A. I. El-Sheikh, "Large-deflection mathematical analysis of rectangular plates," *J. Eng. Mechanics*, **2005**, 131 (8), 809-21.